Novel T-Rail Electrodes for Substrate Removed Low-Voltage High-Speed GaAs/AlGaAs Electrooptic Modulators

JaeHyuk Shin, C. Ozturk, S. R. Sakamoto, Y. J. Chiu, and Nadir Dagli, *Senior Member, IEEE*

***Abstract*—A novel traveling-wave electrode utilizing capacitively loaded T-rail elements was developed for low-voltage high-speed substrate-removed GaAs/AlGaAs electrooptic modulators. Electrodes with varying dimensions were fabricated and characterized. Electrode phase velocity, characteristic impedance, loss coefficient, and capacitive loading were extracted from the measured s-parameters up to 40 GHz. Electrode was also simulated using a finite-element solver. The measured and calculated electrode capacitance values were found to be in excellent agreement, showing that the electrode can be precisely designed. Approaches were outlined to provide a group velocity-matched very high-speed modulator electrode suitable for a low drive-voltage substrate-removed GaAs/AlGaAs electrooptic modulator.**

***Index Terms*—Electrooptic modulators, GaAs modulators, optical modulators, microwave transmission lines.**

I. Introduction

HIGH-SPEED intensity modulated fiber-optic transmission systems require low-voltage high-bandwidth external modulators, preferably with adjustable chirp. Currently, $LiNbO_3$ modulators have the most mature technology and are commercially available [1]. However, there is still need to reduce the drive voltage and improve the frequency response of existing modulators. Modulators in other material systems, such as compound semiconductors and polymers, are actively being researched for this purpose. Compound semiconductor modulators have well-known advantages such as the possibility of integration with sources. They also have other properties that help toward building a superior modulator. Compound semiconductors have very small index dispersion between microwave and optical frequencies. Therefore, in traveling-wave designs, velocity matching requires slowing the microwave signal. This is the opposite of what is required in traveling-wave $LiNbO_3$ modulators. Velocity slowing can be achieved by using capacitively loaded slow-wave electrodes. Such designs allow high electric fields overlapping very well with the optical mode. This possibility combined with the refractive index value higher than $LiNbO_3$ results in a low drive voltage, even in bulk GaAs. Another significant advantage is due to epitaxial growth and advanced processing. For example, using substrate removal techniques, one can process both sides of an epitaxial layer. This enables the fabrication of an ideal push–pull modulator. Taking advantage of these properties, we recently demonstrated a novel substrate-removed (SURE) GaAs/AlGaAs electrooptic modulator [2]. Even with a very conservative design, this device had a drive voltage (V_π) of 8.7 V $\cdot$ cm, which is similar to $LiNbO_3$ modulators. However, the electrode design was not suitable for high-speed operation. Here, we provide the results of the first experimental study of a wide-bandwidth slow-wave electrode that is suitable for high-speed SURE modulators. In Section II, general design guidelines for traveling-wave electrooptic modulators are given. Next, our electrode design that satisfies all these requirements is introduced. This is followed by the description of the fabrication of this electrode and experimental results. Finally, conclusions of this work are presented.

Manuscript received January 5, 2003; revised April 13, 2004.

J. Shin and N. Dagli are with the Electrical Engineering Department, University of California at Santa Barbara, Santa Barbara, CA 93106 USA (e-mail: jhshin@engineering.ucsb.edu; dagli@ece.ucsb.edu).

C. Ozturk was with the Electrical Engineering Department, University of California at Santa Barbara, Santa Barbara, CA 93106 USA. He is now with Sabanci University, 34956 Istanbul, Turkey (e-mail: cemozturk@sabanciuniv.edu)

S. R. Sakamoto was with the Electrical Engineering Department, University of California at Santa Barbara, Santa Barbara, CA 93106 USA. He is now with the Lockheed-Martin Management and Data Systems, San Jose, CA USA (e-mail: steven.r.sakamoto@lmco.com)

Y. J. Chiu was with the Electrical Engineering Department, University of California at Santa Barbara, Santa Barbara, CA 93106 USA. He is now with the National Sun Yat-Sen University, Kaohsiung 804, Taiwan, R.O.C.

Digital Object Identifier 10.1109/TMTT.2004.840735

II. Traveling-Wave Electrooptic Modulator Design Guidelines

For successful utilization of optical modulators in system applications, there is a long list of requirements. This list definitely includes wide bandwidth, low drive voltage, low insertion loss, low wavelength and temperature sensitivity, and low cost. Some of these requirements, such as the drive voltage and bandwidth, are coupled and, usually, compromises are necessary. A well-established approach to very wide electrical bandwidth modulators with low drive voltage is the so-called traveling-wave design. In such a design, the electrode is designed as a transmission line. Therefore, electrode capacitance is distributed and does not create an *RC* limit on the modulator speed. The small-signal modulation response of a traveling-wave modulator whose electrode is terminated by its characteristic impedance is given as [3]

$$M(f) = e^{-\left(\frac{\alpha l}{2}\right)} \left[\frac{\sinh^2\left(\frac{\alpha l}{2}\right) + \sin^2\left(\frac{\xi l}{2}\right)}{\left(\frac{\alpha l}{2}\right)^2 + \left(\frac{\xi l}{2}\right)^2} \right]^{\frac{1}{2}}$$

where

$$\xi = (n_\mu - n_o)\frac{2\pi f}{c}. \tag{1}$$

α and l are the loss coefficient and length of the electrode, respectively. f is the electrical frequency and c is the speed of light in vacuum. n_μ and n_o are the microwave and optical indices and are related to the microwave and optical velocities through well-known expressions. To maximize the bandwidth, microwave and optical velocities should be matched. Our earlier work identified these velocities as the optical group and microwave phase velocity [4], [5]. Based on (1), if there is no velocity mismatch, 3-dB bandwidth will be at the frequency where the total electrode loss becomes 6.34 dB. Therefore, a low-loss and velocity-matched electrode is essential for the realization of a very wide-bandwidth traveling-wave modulator.

The drive voltage V_π of a Mach–Zehnder electrooptic interferometric modulator with push–pull electrodes (in which applied voltage increases the index a certain amount in one arm and decreases exactly the same amount in the other arm of the interferometer) is given as

$$V_\pi = \frac{\lambda}{2l}\frac{t}{n_e^3 r_{41}}\frac{1}{\Gamma} \tag{2}$$

where λ is the wavelength of operation, n_e is the mode effective index, r_{41} is the electrooptic coefficient, t is the electrode gap, and Γ is the overlap between the optical mode and the appropriate component of the applied electric field. For compound semiconductors grown on a (001)-oriented substrate, the appropriate electric-field component is in the (001) direction or perpendicular to the substrate. This electric field modulates the TE polarized optical mode due to bulk electrooptic effect. There is no modulation for the TM polarized optical mode.

Based on this discussion, the following requirements should be satisfied to take full advantage of the traveling-wave idea.

1) Propagation loss of the optical guide should be low so that a long modulator can be realized. This helps to significantly reduce the drive voltage, as seen in (2).
2) Electrode phase velocity should be matched to optical group velocity. The electrodes should not have dispersion; in other words, the electrode group and phase velocities should be the same. This eliminates the velocity mismatch and the electrode can be made very long. In III–V semiconductors, velocity matching requires slowing the microwave velocity.

   Optical group velocity v_g, which is the target electrode phase velocity $v_{\rm ph}$ is known for a given material system. For example, GaAs/AlGaAs material system at 1.55 μm has a group index around 3.5, which corresponds to

$$v_g = \frac{30}{3.5} = 8.57 \text{ cm/ns}. \tag{3}$$

   Furthermore, if the desired electrode characteristic impedance is Z_0, the capacitance per unit length C and inductance per unit length L of the electrode can be expressed using the well-known transmission-line equations as

$$v_{\rm ph} = \sqrt{\frac{1}{LC}}$$
$$Z_0 = \sqrt{\frac{L}{C}}$$

   as

$$C = \frac{1}{Z_0 v_{\rm ph}}$$
$$L = \frac{Z_0}{v_{\rm ph}}. \tag{4}$$

   As an example, assume a 50-Ω electrode with 8.57-cm/ns phase velocity. The required C and L values are then

$$C = 2.3 \text{ pF/cm and } L = 5.8 \text{ nH/cm}. \tag{5}$$

3) Electrode microwave loss coefficient should be low so that a long modulator can be realized. As described earlier, total electrode loss should be lower than 6.34 dB at the desired 3-dB bandwidth point.
4) For efficient modulation, a good overlap between the optical mode and vertical component of the microwave electric field is needed. In other words, Γ in (2) should be as close to one as possible.
5) Push–pull drive should be possible to reduce the drive voltage a factor of two. This also makes chirp zero.
6) Electrode gap t should be as small as possible to generate as large an electric field as possible for a given voltage. However, this should be achieved without making electrode capacitance and loss, as well as optical loss, excessively large.
7) The electrooptic coefficient r_{41} should be increased as much as possible without increasing optical loss.

Conditions 1) and 3) are hard to realize when doped layers are present. One can reduce the optical and microwave loss drastically using unintentionally doped self-depleting GaAs/AlGaAs layers, as we demonstrated earlier [6], [8]. Using undoped layers makes condition 4) difficult to realize unless the growth substrate is removed. By removing the growth substrate, independent electrodes can be placed directly on the top and bottom of an optical waveguide. This makes it possible to apply a (001)-oriented electric field overlapping very well with the optical mode. Conditions 5) and 6) are also difficult to realize in an optimum way if the high dielectric constant growth substrate is present. If the substrate is removed, the electrodes at the top and bottom of the optical waveguide can be independently biased. This allows applying the same voltage magnitude with opposite polarity across the arms of an interferometer, and the direction of the electric field between the arms can easily be reversed. Hence, true push–pull operation can be realized. If the substrate were present, changing the electric-field direction between the arms would require a biasing scheme, which doubles the voltage required [14]. Furthermore, the electrode gap becomes the same as the epilayer thickness, hence, it can easily be reduced significantly. Therefore, for a given voltage, the vertical component of

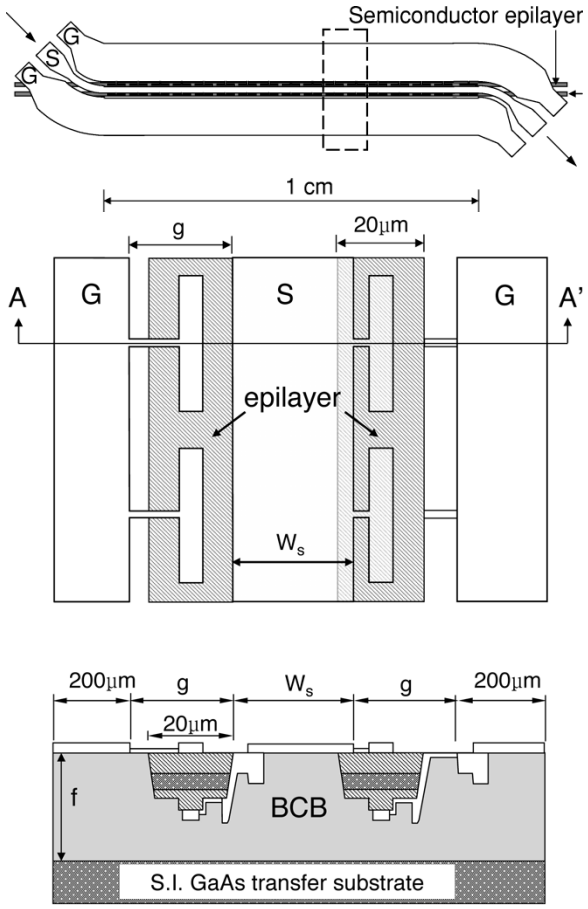

Fig. 1. Top longitudinal schematic of the electrode and details of its top and cross-sectional profiles.

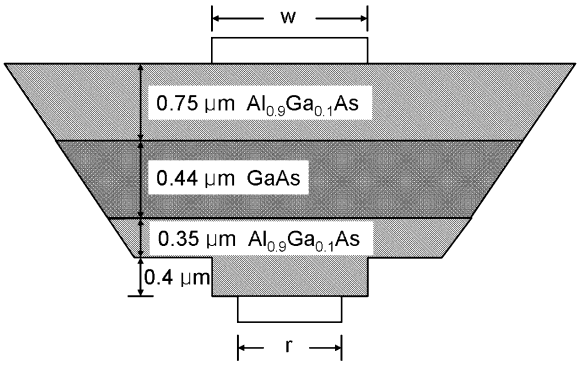

Fig. 2. Cross-sectional profile of the optical waveguide with top and bottom rails.

the electrical field is maximized. Condition 7) can be realized by using quantum wells of appropriate composition. In this study, we present an electrode design to satisfy all these requirements, except for condition 7), and yield modulators with superior characteristics. However, the given electrode can also be used with an appropriate material design satisfying condition 7).

III. Device Description

Figs. 1 and 2 show the details of the top and cross-sectional views of the microwave electrode, respectively. The electrode is

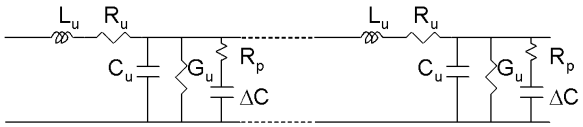

Fig. 3. Electrical equivalent circuit of the electrode.

a ground–signal–ground (G–S–G) coplanar waveguide periodically loaded by tiny capacitors. The unloaded line is formed on a polymer layer, which is on a transfer substrate. In this case, the polymer and transfer substrate are benzocylcobutene (BCB) and semi-insulating (SI) GaAs, respectively. The tiny capacitors that periodically load the unloaded line are formed in between the "T-rails" placed on the top and bottom of each single-mode semiconductor waveguide, as shown in Fig. 1. The two waveguides form the arms of a Mach–Zehnder-type modulator. These waveguides are formed on an epilayer removed from its growth substrate. Such SURE waveguides with very low optical propagation loss were realized earlier, as both stand alone waveguides [6] or as parts of SURE modulators [2]. The topside and backside T-rails are connected to the signal and ground electrodes of the unloaded line using narrow stems, respectively. In this design, epilayer thickness is the same as the electrode gap. Hence, very accurately controlled narrow electrode gaps are possible. The periodical loading of the unloaded line with these tiny capacitors form a slow-wave transmission line [7]. The equivalent circuit of the resulting electrode is shown in Fig. 3. L_u, C_u, R_u, and G_u are the inductance, capacitance, resistance, and conductance per unit length of the unloaded transmission line. ΔC is the capacitance per unit length due to capacitive loading on one arm of the modulator, and R_p is due to the resistance of the stems. One can express ΔC as

$$\Delta C = K\frac{\varepsilon_{\mathrm{GaAs}} r}{t} F \quad F = \frac{p}{d} \tag{6}$$

where r is the width of the topside rail, t is the overall thickness of the epilayer, p is the length of the rails, $d = l/N$ is the period of the loading, l is the length of the electrode, N is the number of periods, and F is the fill factor. K is a scaling factor that accounts for the fringing fields as well as the geometrical details of the epilayer between the rails.

We previously used such capacitively loaded slow-wave electrodes in the design and fabrication of traveling-wave electrooptic modulators [8], [9]. Our previous results indicate that periodic loading is mainly capacitive and the inductance per unit length of the loaded line is almost identical to that of the unloaded line. We can then express the characteristic impedance Z_0 and the phase velocity v_{ph} of the loaded line as

$$Z_0 = \sqrt{\frac{L_u}{(C_u + 2\Delta C)}} \text{ and } v_{\mathrm{ph}} = \sqrt{\frac{1}{L_u(C_u + 2\Delta C)}}. \tag{7}$$

The target value of Z_0 is typically $50\,\Omega$. v_{ph} should be chosen as the optical group velocity of the semiconductor optical waveguide. If the value of ΔC is known, one can choose a suitable unloaded line geometry with the required L_u and C_u values.

The first step in the design is to choose the appropriate epilayer. To keep V_π as low as possible, t should be kept as small as possible, as seen in (2). This requires tight vertical confinement, which is achieved by maximizing the index step between the core and upper and lower claddings of the optical waveguide. In a GaAs/AlGaAs material system, this can be achieved by choosing the core as GaAs and the Al content of the claddings as high as possible. This choice also helps to reduce ΔC since high Al-content AlGaAs layers have a lower dielectric constant. In our design, the upper and lower claddings are chosen as $Al_{0.9}Ga_{0.1}As$. The core and cladding thicknesses are then chosen such that optical mode is entirely confined in the semiconductor layers and the overlap of the optical mode with the metal electrodes is minimized. This is essential to minimize the optical propagation loss. This condition is achieved by choosing the core layer as thick as possible to increase the confinement. The upper limit is the cutoff thickness of the second-order TE slab mode. The cladding thickness is then increased until the overlap of the optical mode with the metal layers is minimized. The criterion for the minimum overlap value is found considering the optical propagation loss due to metal electrodes. This loss is calculated using the complex refractive index of the metal and a perturbation analysis. An excess optical propagation loss of 0.1 dB/cm was used as the criteria. The resulting epitaxial design is shown Fig. 2. It has a 0.44-μm-thick GaAs core layer surrounded by 0.75-μm-thick $Al_{0.9}Ga_{0.1}As$ upper and lower claddings. The next step is to choose the width of the rib waveguide. This value was chosen as 4 μm, mainly due to lithographic considerations. Once the width is determined, the etch depth of the rib for single-mode operation can be calculated. The first cut calculation was done using the effective dielectric-constant method, which gives a conservative estimate. The value found this way was verified using beam propagation method analysis. The result was a rib etch of 0.4 μm. Once the epi thickness and waveguide width were determined, the T-rail capacitance ΔC was estimated using (6) with $K = 1$ and different T-rail widths. For a given T-rail width, this value defines the upper limit since the effect of rib etching and the lower dielectric constant of upper and lower claddings are not taken into account. Once this value was estimated, capacitance and inductance per unit length of the unloaded line were calculated using (7). The values were then converted into line dimensions using well-known transmission-line design equations [10]. This exercise resulted in different line dimensions. Using these calculations, we determined a parameter space to experimentally determine the optimum electrode geometry. We used two different topside rail widths of $r = 1.5$ μm and 3 μm. The bottom rails widths corresponding to these top rail widths were chosen as 2 and 4 μm, respectively. The period of loading was chosen as 100 μm. Since a slow-wave transmission line also works as a filter, we need to make the Bragg frequency as high as possible so as not to have a dispersive electrode. This choice makes the Bragg frequency in the several hundred gigahertz range [11], hence, there are no dispersive effects in the range of frequencies investigated in this study. We kept the fill factor F at 0.9 to keep the drive voltage as low as possible. The width of the signal line W_s was chosen as 40 μm. A wider center conductor results in a lower microwave loss, but increases the unloaded line capacitance. Furthermore, a wider center conductor requires further separation between the arms of the interferometer. This results in longer Y-branches to keep the optical loss minimum, which makes the device longer. 40 μm was estimated to be a reasonable compromise. The main electrode gap g was chosen as 80 μm mainly to reduce the unloaded line capacitance as much as possible.

IV. Device Fabrication

Fabrication steps are shown in Fig. 4. Fabrication starts with the molecular beam epitaxy (MBE) growth of the designed epilayer. This epilayer is unintentionally doped and is self depleting due to Fermi level pinning at the surfaces. This results in very low conductivity and the entire epilayer behaves as a dielectric with slight loss for alternating fields of frequency in excess of 10 Hz [2]. Next, the 4-μm-wide waveguides were fabricated using reactive ion etching (RIE) of the semiconductor in a $BCl_3/SiCl_4$ gas mixture. The resultant profile at the end of this step is shown in Fig. 4(a). The etch mask used was hard-baked photoresist and the etch depth was 0.4 μm. This was followed by topside electrode fabrication. The process was done in two steps. First, T-rails with short stems were fabricated using liftoff, as shown in Fig. 4(b). The metal used in this step was 200 Å Ti/5000 Å Au evaporated by e-beam, which formed Schottky contacts. The epilayer was then etched in the field regions slightly into the AlAs etch stop layer, as shown in Fig. 4(c), using a mixture of $H_3PO_4 : H_2O_2 : H_2O = 1 : 14 : 200$. This step removed the epilayer, except for the areas where optical guiding is needed. The wet etch also gave sloped sidewalls, which ensured that the connecting partial electrodes would not break when going over the mesa etch. The next step was to form the partial electrodes, which connect the front T-rails to the back electrodes. These partial electrodes were formed using liftoff. In order to obtain good liftoff, a thick deep UV photoresist known as SF-11 was used to planarize the uneven surface. Regular photoresist was spun on the 2.5-μm-thick SF-11 layer and was patterned using regular photolithography. The patterned photoresist was used as a mask to expose SF-11 under a deep UV light source. After developing SF-11, 200-Å Ti/15 000-Å Au was deposited by e-beam. An overnight bath in the SF stripper lifted off the patterns, as shown in Fig. 4(d). The epilayer was then transferred to another GaAs substrate using a BCB layer as glue. This was followed by spray etching the growth substrate. The details of this process were outlined in [2] and [6]. With the removal of the growth substrate, processing of the backside epilayer was possible. Using standard lithography, the backside T-rails and electrodes were patterned using liftoff. The electrode was 200-Å Ti/5000-Å Au evaporated by e-beam, which formed Schottky contacts. Separate microwave calibration standards were also fabricated. A 6-μm-thick BCB layer was spun and cured on a piece of SI GaAs substrate and 200-Å Ti/5000-Å Au calibration standards were patterned using the standard liftoff technique.

V. Experimental Results

Microwave measurements were made using the HP8510 vector network analyzer. Using a thru-reflect-line (TRL) microwave calibration scheme, the input/output probe pads

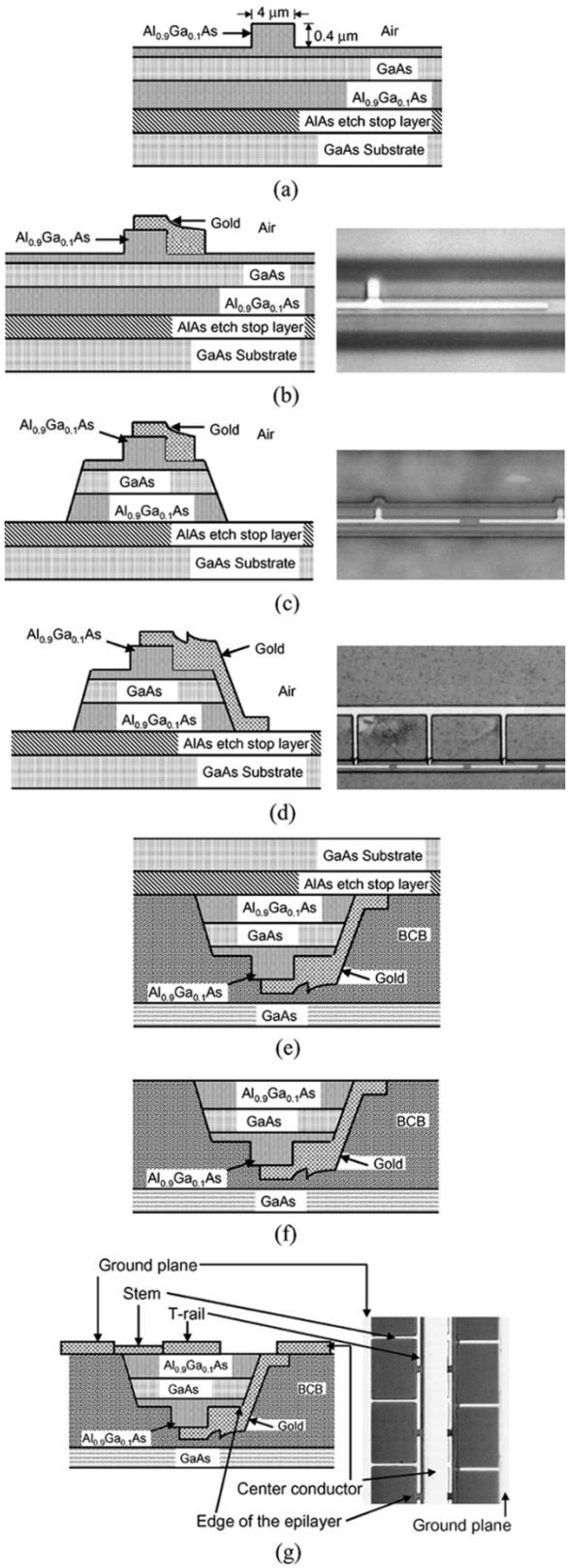

Fig. 4. Processing steps used in the fabrication. (a) Waveguide etch. (b) Deposition of the top rails. (c) Removal of the epitaxial layer where not needed. (d) Deposition of the partial electrode. (e) Gluing of the device onto a transfer substrate. (f) Substrate removal. (g) Deposition of the bottom rails and the rest of the electrode.

were calibrated out. A typical plot for the s_{11}- and s_{12}-parameters is shown in Fig. 5.

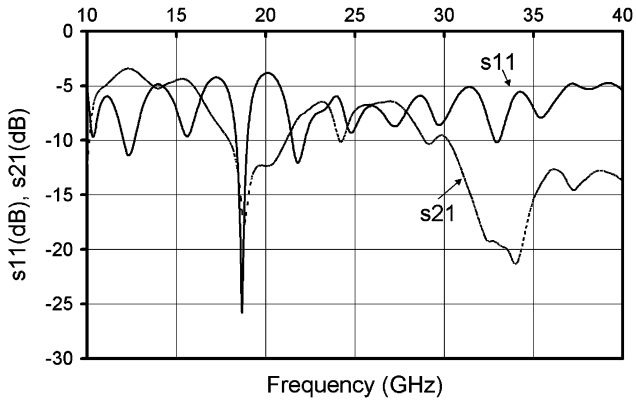

Fig. 5. Measured s-parameters for the electrode with $r = 3\ \mu$m and $w = 4\ \mu$m. The reference impedance level for the measurements was 94 Ω.

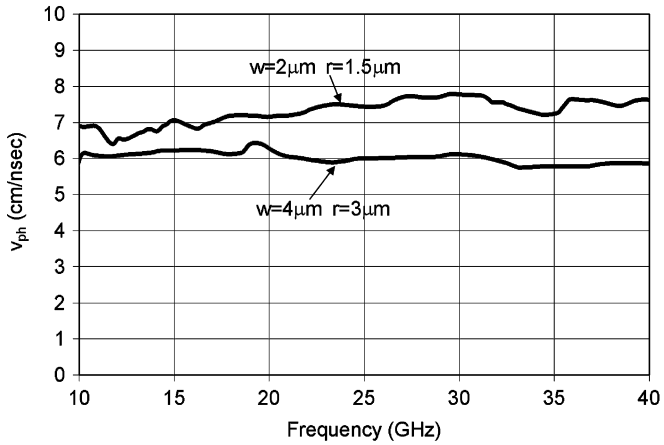

Fig. 6. Phase velocity $v_{\rm ph}$ calculated directly using the s-parameters for two different rail dimensions.

One technique to determine the line parameters is to convert the measured s-parameters into $ABCD$-parameters and then use these $ABCD$-parameters to calculate the microwave phase velocity $v_{\rm ph}$, microwave loss α, and the loaded line characteristic impedance Z_0 [12]. The loaded line capacitance C and inductance L can be found from $v_{\rm ph}$ and Z_0. We will refer to this as the direct extraction technique. The results obtained this way are shown in Fig. 6.

$v_{\rm ph}$ was found to be 6.0±0.4 cm/ns and 7.2±0.6 cm/ns for T-rail width combinations of ($r = 3\ \mu$m, $w = 4\ \mu$m) and ($r = 1.5\ \mu$m, $w = 2\ \mu$m), respectively. However, a reliable value of Z_0 could not be extracted by this procedure. Z_0 is very sensitive to reflection s-parameters s_{11} and s_{22}, which are relatively weak. Even a small change in the s_{11}- and s_{22}-parameters due to resonances originating from small reflections shifts the measured Z_0 around the true value considerably. However, we can obtain the crucial parameters as follows. The unloaded line inductance L_u and unloaded line capacitance C_u was calculated to be $L_u = 5.987$ nH/cm and $C_u = 0.673$ pF/cm for electrodes sitting on 9.2-μm-thick BCB on SI GaAs using a previously developed program [13]. It was also previously found that the inductance is almost exactly the same for loaded and unloaded structures [8]. Thus, assuming that the loaded line inductance is the same as the unloaded line inductance, one can determine the

TABLE I
SUMMARY OF RESULTS OBTAINED USING THE DIRECT EXTRACTION TECHNIQUE

T-rail dimension	v_{ph}	ΔC	ΔC (theory)	Z_0	Z_0 (theory)
w = 4 μm, r = 3 μm	6.0±0.4 cm/ns	2.02±0.32 pF/cm	2.02 pF/cm	35.9±2.5 Ω	35.6 Ω
w = 2 μm, r = 1.5 μm	7.2±0.6 cm/ns	1.30±0.27 pF/cm	1.26 pF/cm	43.1±3.6 Ω	43.3 Ω

additional capacitance per arm ΔC due to the T-rails using (7) as

$$\Delta C = \frac{1}{2}\left(\frac{1}{L_u v_{\rm ph}^2} - C_u\right). \tag{8}$$

Once ΔC is found, the impedance of the loaded line Z_0 can be calculated using (7). Table I shows the results obtained this way for different T-rail dimensions.

A different approach was also used to determine $v_{\rm ph}$ and Z_0. One can convert the s-parameters to $ABCD$-parameters using the well-known expressions. $ABCD$-parameters are related to the complex propagation constant γ and characteristic impedance Z_0 through

$$\begin{aligned} |A| &= \left|\cosh(\gamma l)\right| \\ &= \left|\cosh\left((\alpha + j\beta)l\right)\right| \\ &= \sqrt{\frac{1}{2}\left[\cosh(2\alpha l) + \cos(2\beta l)\right]} \end{aligned} \tag{9}$$

$$\begin{aligned} |B| &= \left|Z_0 \sinh(\gamma l)\right| \\ &= Z_0\sqrt{\frac{1}{2}\left[\cosh(2\alpha l) - \cos(2\beta l)\right]} \end{aligned} \tag{10}$$

Furthermore, γ can be written as

$$\gamma = \sqrt{(R + j2\pi f L)(G + j2\pi f C)} = \alpha + j\beta$$

with

$$R = a \cdot f^b \text{ and } v_{\rm ph} = \frac{2\pi f}{\beta}. \tag{11}$$

Equations (9)–(11) were fitted to the experimental data using a, b, L, G, and C as fitting parameters. Once the fitting parameters are found, the line parameters can be calculated using (4) and (11). We refer to this as the curve-fitting technique. Fig. 7 shows the directly extracted and the curve-fitted $|A|$ using this technique. The fit is quite good up to 30 GHz. The frequency variation of the line parameters obtained this way is shown in Fig. 8 and the results are summarized in Table II.

As expected, narrower rails have smaller loading capacitance. This results in less velocity slowing and higher characteristic impedance. The microwave loss is mainly due to the conductor loss of the unloaded line. The additional resistance due to stems increases the loss slightly. In this case, the loss coefficient is high since the electrode metal is only 0.5-μm thick. This loss can be reduced significantly by increasing the metal thickness.

The resonances in the s-parameters proved to be detrimental in obtaining a better fit, as well as directly extracting Z_0. They arise due to reflections in the electrode. Calibration should help to reduce the effect of reflections up to the reference planes. The resonances due to reflections at the reference planes are spaced

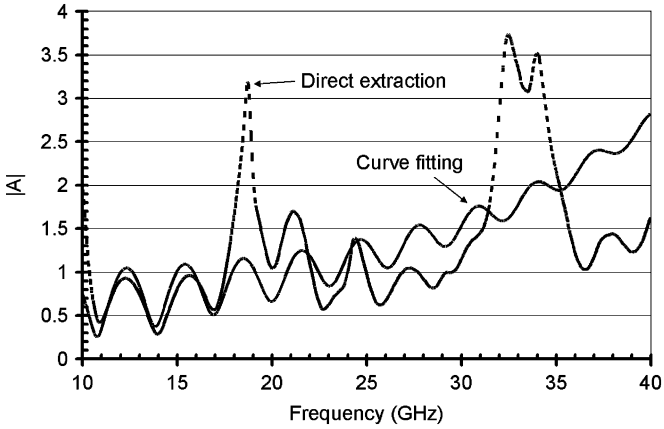

Fig. 7. Experimental and fitted value of $|A|$ as a function of frequency obtained using the curve-fitting technique.

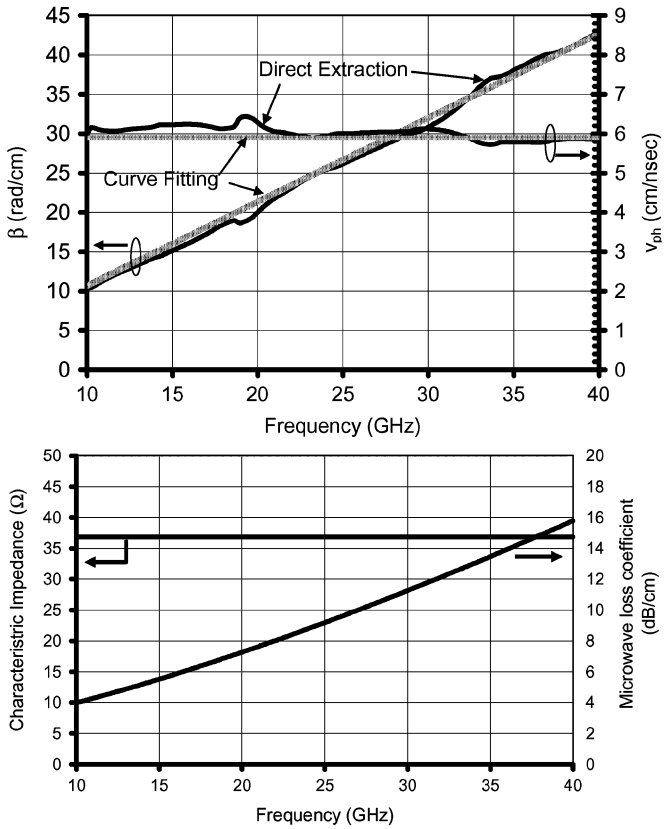

Fig. 8. Frequency variation of phase velocity $v_{\rm ph}$, characteristic impedance Z_0, microwave loss coefficient α, and phase constant β obtained using the curve-fitting technique. $v_{\rm ph}$ and β values directly extracted from the measured s-parameters are also shown. In this case, $r = 3$ μm and $w = 4$ μm.

TABLE II
SUMMARY OF THE RESULTS OBTAINED USING THE CURVE-FITTING TECHNIQUE

T-rail dimension	v_{ph}	ΔC	Z_0
w = 4 μm, r = 3 μm	5.9 cm/ns	2.06 pF/cm	36.8 Ω
w = 2 μm, r = 1.5 μm	7.1 cm/ns	1.28 pF/cm	43.4 Ω

approximately 3 and 3.5 GHz depending on T-rail dimensions. However, additional resonances were also observed. These additional resonances are thought to originate from the GaAs epilayer underneath the electrode. The electrode turns 45° away at both ends to minimize the overlap of the probe pads with optical waveguides at the input and output. The electrode in the bent section is on top of the BCB. However, there is a small region between the probe pads and main electrode where the electrode crosses over the semiconductor epilayer, as shown in Fig. 1. This creates a big dielectric constant step and, thus, reflections, which is thought to be the source of additional resonances appearing in the s-parameters. Since calibration standards did not include the epilayers, it was not possible to calibrate out these reflections. They can be calibrated out using a calibration standard with epilayers buried in the BCB. Alternatively, one can reduce these reflections by tapering the epilayer in such a way that the microwave field gradually "feels" the epilayer, hence, reducing sharp reflections.

The modeling was also used to calculate the measured parameters. As described earlier, unintentionally doped semiconductor epilayer behaves as a slightly lossy dielectric at frequencies over a few hertz. Schottky electrodes can then be modeled as regular electrodes on dielectric material. Hence, we can carry out a quasi-static analysis by numerically solving the Laplace's equation for the given geometry. In the solutions, a commercially available software package was used.[1] This package allows an adaptive finite-element solution, which allowed us to model the entire electrode accurately. Fig. 9 shows the overall mesh and the mesh in between the T-rails. As seen in this figure, a submicrometer mesh was possible over the optical waveguide, where the electric field is the highest. The resulting electrostatic potential distribution on the optical waveguide is shown in Fig. 10. Once the potential was found, the total charge on the electrode and line capacitance was calculated. Subtracting the unloaded line capacitance from the total electrode capacitance, dividing by 2, and multiplying by 0.9 to account for the fill factor, ΔC was obtained. The calculated values were listed along with the experimental values in Table I. The agreement between the experimental values deduced using two different techniques and the calculated value are excellent. These results show that we can design the appropriate electrode very accurately.

It is obvious that the additional capacitance due to the T-rails is too high, which lowered the values of Z_0 and $v_{\rm ph}$ below their target values of 50 Ω and 8.57 cm/ns. There are three approaches to reduce this value. One is to reduce the length of the T-rails. However, this comes at the expense of reduced effective electrode length, which means the drive voltage will be higher. The second approach is to reduce the unloaded line capacitance. This can be done using a low dielectric-constant substrate such as quartz and/or increasing the low dielectric-constant polymer bonding layer thickness. However, since the rail capacitance is almost the same as the desired capacitance per unit length value, shown in (5), this approach only helps to improve Z_0 and $v_{\rm ph}$ values somewhat. The third approach could be to reduce ΔC by reducing the width of the rails. This is clearly demonstrated in Tables I and II. However, to maintain a good overlap with the optical mode, the width of the optical waveguide should also be reduced. This requires a more strongly confined waveguide, which can be fabricated using substrate removal techniques. Using a combination of these three approaches, an optimum design could be possible. However, even with the current design, one can still match the velocity at the expense of electrode impedance. This requires reducing the inductance of the unloaded line. This may not be a bad compromise provided that the electrode can be terminated with a matched termination. For example, using $\Delta C = 1.3$ pF/cm as determined in this experiment [see (4) and (7)] and assuming that the velocity of the unloaded coplanar line is

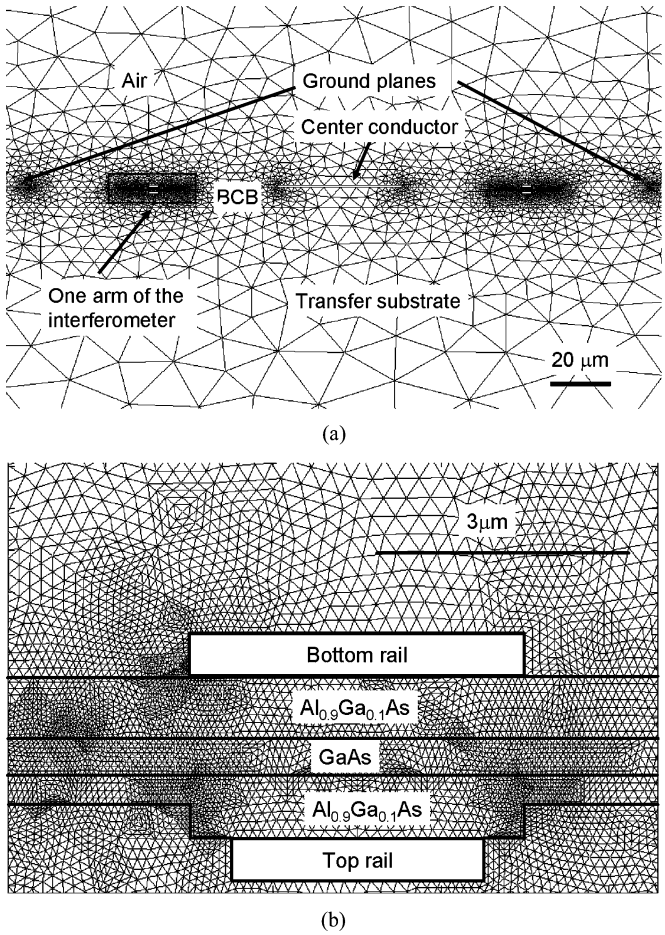

Fig. 9. Adaptive mesh used in the simulations: (a) over the entire electrode and (b) over the optical waveguide.

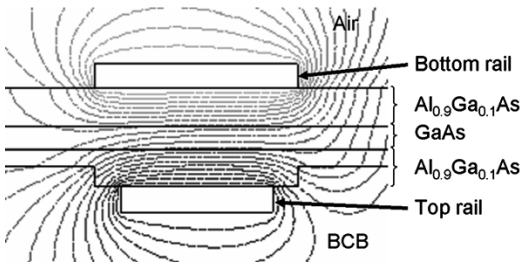

Fig. 10. Electrostatic potential over the optical waveguide.

[1]MATLAB Partial Differential Equations Toolbox, The Mathworks, Natick, MA.

given as $v_{\rm ph} = c/\sqrt{(\varepsilon_r + 1)/2}$, we can calculate C_u and L_u values under the velocity matching condition. This, in turn, allows us to calculate the Z_0 value. In this calculation, if we assume $\varepsilon_r = 13$, i.e., without polymer bonding layer, we obtain $Z_0 \approx 18\ \Omega$. If we use this velocity-matched 18-Ω electrode with a matched termination, there will not be a standing wave on the line. Even if this electrode is driven by a 50-Ω source, 76% of the available power from the source will be transferred to the electrode. This is the worst case estimate, and using the techniques outlined above, a more favorable situation can be obtained.

In this electrode study, there was not a full modulator since input and output Y-branches were missing. However, the V_π of a full modulator can be estimated using (2) for the waveguide design shown in Fig. 2. Using $\Gamma = 0.7$ and $n_e = 3.3, r_{41} = 1.6 \times 10^{-12}$ m/V, $t = 2\ \mu$m at 1.5 μm, one obtains a V_π of 3.7 V $\cdot$ cm.

VI. Conclusion

In this paper, a novel capacitively loaded T-rail electrode for low-voltage high-speed SURE GaAs/AlGaAs electrooptic modulators has been designed, fabricated, and characterized up to 40 GHz. The electrode design satisfies all the requirements of a traveling-wave electrode suitable for a low-voltage and high-speed electrooptic modulator. Measured values of electrode impedance, loss coefficient, phase velocity, and capacitive loading were provided for different line dimensions using two different data extraction techniques. The capacitive loading was found to be higher than desired, which resulted in lower than desired characteristic impedance and phase velocity. However, the measured capacitance values are in excellent agreement with the results of simulations, showing that this type of a modulator can be precisely designed. Different approaches were outlined to reduce the capacitive loading. The results along with the ability to accurately simulate make this electrode suitable for low-voltage high-speed GaAs/AlGaAs electrooptic modulators.

References

[1] N. Dagli, "Wide bandwidth lasers and modulators for RF photonics," *IEEE Trans. Microw. Theory Tech.*, vol. 47, no. 7, pp. 1151–1171, Jul. 1999.

[2] S. R. Sakamoto, A. Jackson, and N. Dagli, "Substrate removed GaAs/AlGaAs electrooptic modulators," *IEEE Photon. Technol. Lett.*, vol. 11, no. 10, pp. 1244–1246, Oct. 1999.

[3] K. Kubota, J. Noda, and O. Mikami, "Traveling wave optical modulator using a directional coupler $LiNbO_3$ waveguide," *IEEE J. Quantum Electron.*, vol. QE-16, no. 7, pp. 754–760, Jul. 1980.

[4] R. Spickermann, S. R. Sakamoto, and N. Dagli, "In traveling wave modulators which velocity to match," in *Proc. 9th Annu. IEEE/LEOS'96 Meeting*, Boston, MA, Nov. 18–21, 1996, Paper WM3, pp. 97–98.

[5] R. Spickermann, S. R. Sakamoto, and N. Dagli, "GaAs/AlGaAs traveling wave electrooptic modulators," in *Proc. SPIE Optoelectronic Integrated Circuits Conf.*, vol. 3006, San Jose, CA, Feb. 8–14, 1997, Paper 33, pp. 272–279.

[6] S. R. Sakamoto, C. Ozturk, Y. T. Byun, J. Ko, and N. Dagli, "Low loss substrate-removed (SURE) optical waveguides in GaAs/AlGaAs epitaxial layers embedded in organic polymers," *IEEE Photon. Technol. Lett.*, vol. 10, no. 7, pp. 985–987, Jul. 1998.

[7] R. E. Collin, *Foundations for Microwave Engineering*. New York: McGraw-Hill, 1966.

[8] S. R. Sakamoto, R. Spickermann, and N. Dagli, "Narrow gap coplanar slow wave electrode for travelling wave electro-optic modulators," *Electron. Lett.*, vol. 31, no. 14, pp. 1183–1185, Jul. 1995.

[9] R. Spickermann, S. R. Sakamoto, M. G. Peters, and N. Dagli, "GaAs/AlGaAs travelling wave electrooptic modulators with an electrical bandwidth >40 GHz," *Electron. Lett.*, vol. 32, no. 12, pp. 1095–1096, Jun. 1996.

[10] K. Gupta, R. Garg, I. Bahl, and P. Bhartia, *Microstrip Lines and Slotlines*. Norwood, MA: Artech House, 1996.

[11] R. Spickermann and N. Dagli, "Experimental analysis of millimeter wave coplanar waveguide slow wave structures on GaAs," *IEEE Trans. Microw. Theory Tech.*, vol. 42, no. 10, pp. 1918–1924, Oct. 1994.

[12] K. Kiziloglu, N. Dagli, G. L. Matthaei, and S. I. Long, "Experimental analysis of transmission line parameters in high-speed GaAs digital circuit interconnects," *IEEE Trans. Microw. Theory Tech.*, vol. 39, no. 8, pp. 1361–1367, Aug. 1991.

[13] G. L. Matthaei, G. Chinn, C. Plott, and N. Dagli, "A simplified means for computation of interconnect distributed capacitances and inductances," *IEEE Trans. Computer-Aided Design Integr. Circuits Syst.*, vol. 11, no. 4, pp. 513–524, Apr. 1992.

[14] R. G. Walker, "High speed III–V semiconductor intensity modulators," *IEEE J. Quantum Electron.*, vol. 27, no. 3, pp. 654–667, Mar. 1991.

JaeHyuk Shin was born on February 4, 1975, in Seoul, Korea. He received the B.S. degree in inorganic materials engineering from Seoul National University, Seoul, Korea, in 1999, and is currently working toward the M.S./Ph.D. degree in materials from the University of California at Santa Barbara. His graduate studies focus on the development of high-bandwidth low-drive voltage modulators for fiber-optic communications.

C. Ozturk, photograph and biography not available at time of publication.

S. R. Sakamoto, photograph and biography not available at time of publication.

Y. J. Chiu, photograph and biography not available at time of publication.

Nadir Dagli (M'79–SM'04) was born in Ankara, Turkey. He received the B.S. and M.S. degrees in electrical engineering from the Middle East Technical University, Ankara, Turkey, in 1976 and 1979, respectively, and Ph.D. degree in electrical engineering from the Massachusetts Institute of Technology (MIT), Cambridge, in 1986.

Upon graduation, he joined the Electrical and Computer Engineering Department, University of California at Santa Barbara, where he is currently a Professor. He has authored or coauthored over 100 refereed journal and conference publications. His current interests are design, fabrication, and modeling of guided-wave components for optical integrated circuits, ultrafast electrooptic modulators, wavelength division multiplexing (WDM) components, and photonic nanostructures.

Dr. Dagli is currently editor for IEEE Photonics Technology Letters and is an elected member of the IEEE Lasers and Electro-Optics Society (LEOS) Board of Governors.